



**HAL**  
open science

## Extended Investigations on Luminescent s<sub>2</sub>[Mo<sub>6</sub>Br<sub>14</sub>]*@*SiO<sub>2</sub>Nanoparticles: Physico-Structural Characterizations and Toxicity Studies

Tangi Aubert, Francisco Cabello-Hurtado, Marie-Andrée Esnault, Chrystelle Neaime, Dominique Lebret-Chauvel, Sylvie Jeanne, Pascal Pellen, Claire Roiland, Laurent Le Pollès, Noriko Saito, et al.

### ► To cite this version:

Tangi Aubert, Francisco Cabello-Hurtado, Marie-Andrée Esnault, Chrystelle Neaime, Dominique Lebret-Chauvel, et al.. Extended Investigations on Luminescent s<sub>2</sub>[Mo<sub>6</sub>Br<sub>14</sub>]*@*SiO<sub>2</sub>Nanoparticles: Physico-Structural Characterizations and Toxicity Studies. *Journal of Physical Chemistry C*, 2013, 117 (39), pp.20154-20163. 10.1021/jp405836q . hal-00907963

**HAL Id: hal-00907963**

**<https://hal.science/hal-00907963>**

Submitted on 22 Oct 2021

**HAL** is a multi-disciplinary open access archive for the deposit and dissemination of scientific research documents, whether they are published or not. The documents may come from teaching and research institutions in France or abroad, or from public or private research centers.

L'archive ouverte pluridisciplinaire **HAL**, est destinée au dépôt et à la diffusion de documents scientifiques de niveau recherche, publiés ou non, émanant des établissements d'enseignement et de recherche français ou étrangers, des laboratoires publics ou privés.

# Extended Investigations on Luminescent $\text{Cs}_2[\text{Mo}_6\text{Br}_{14}]\text{@SiO}_2$ Nanoparticles: Physico-Structural Characterizations and Toxicity Studies

Tangi Aubert,<sup>†‡\*</sup> Francisco Cabello-Hurtado,<sup>‡</sup> Marie-Andrée Esnault,<sup>‡</sup> Chrystelle Neaime,<sup>†</sup> Dominique Lebret-Chauvel,<sup>†</sup> Sylvie Jeanne,<sup>†</sup> Pascal Pellen,<sup>†</sup> Claire Roiland,<sup>†</sup> Laurent Le Polles,<sup>†</sup> Noriko Saito,<sup>§</sup> Koji Kimoto,<sup>§</sup> Hajime Haneda,<sup>§</sup> Naoki Ohashi,<sup>§</sup> Fabien Grasset,<sup>†\*</sup> Stéphane Cordier<sup>†\*</sup>

<sup>†</sup> University of Rennes 1, UMR UR1-CNRS 6226 Institut des Sciences Chimiques de Rennes, Solid State Chemistry and Materials Group, 263 av. du Général Leclerc, 35042 Rennes, France.

<sup>‡</sup> University of Rennes 1, UMR UR1-CNRS 6553 Ecobio, Mechanisms at the Origin of Biodiversity Team, University of Rennes 1, 263 av. du Général Leclerc, 35042 Rennes, France.

<sup>§</sup> National Institute for Materials Science, 1-1 Namiki, Tsukuba, Ibaraki 305-044, Japan.

---

**ABSTRACT:** Functional silica nanoparticles and in particular luminescent silica nanoparticles constitute very promising candidates for many applications in the field of biotechnology, theranostics and photonics. However, optimizing the design of such materials requires a deep understanding of their physico-chemical properties. In this article are reported extended investigations on luminescent  $\text{Cs}_2[\text{Mo}_6\text{Br}_{14}]\text{@SiO}_2$  nanoparticles prepared by a water-in-oil microemulsion technique. We bring here new insights into the structure of such nanoparticles and its interplay with their optical properties. The structural interactions between the cluster units and the silica matrix were investigated and are discussed in details on the basis of FE-SEM, HAADF-STEM, ICP-OES, BET,  $^{29}\text{Si}$  MAS NMR and photoluminescence studies. As part of the risk evaluation before potential applications, the toxicity of the nanoparticles both on plants and on human cells was evaluated.

---

**KEYWORDS:** silica nanoparticles, metal atom clusters, luminescence, theranostics, hybrid materials.

## 1. Introduction

Luminescent silica nanoparticles find numerous applications in the fields of biotechnologies<sup>1,2</sup> or photonics.<sup>3,4</sup> They are usually achieved through the encapsulation of luminophores such as organic dyes,<sup>5-8</sup> semi-conductor quantum dots,<sup>9-13</sup> organometallic complexes<sup>14-16</sup> or doped nanocrystals.<sup>17-20</sup> Molecular luminophores such as organic dyes and organometallic complexes can be covalently bonded to the silica matrix by prior functionalization with organosilanes.<sup>21-23</sup> Ma *et al.* studied the influence of the type of interaction between organic dyes and the silica matrix on the luminescence properties of the resulting material.<sup>24</sup> They showed that a covalent interaction can enhance the luminescence quantum yield of the nanoparticles. In addition, strong interactions will ensure a better overall physico-chemical stability of the system. Thus, understanding the interactions between the

luminophores and the matrix is a key point in the fabrication and optimization of luminescent silica nanoparticles.

In the past few years, we reported luminescent silica nanoparticles through the encapsulation of  $\text{Mo}_6$ -based and  $\text{Re}_6$ -based transition metal atom clusters by water-in-oil microemulsion processes.<sup>25-27</sup> These cluster units have also been associated with magnetic  $\gamma\text{-Fe}_2\text{O}_3$  nanocrystals to produce bi-functional luminescent and magnetic nanoparticles.<sup>28</sup>  $[\text{M}_6\text{X}_8\text{Y}^a_6]^{n-}$  nanosized cluster units are built up from an octahedral  $\text{M}_6$  cluster ( $\text{M} = \text{Mo}$  or  $\text{Re}$ ) bonded to eight inner face-capping ligands ( $\text{X}^i$ ,  $i = \text{inner}$ ,  $\text{X} = \text{Cl}$ ,  $\text{Br}$ ,  $\text{I}$ ,  $\text{S}$  or  $\text{Se}$ ) and to six apical ligands ( $\text{Y}^a$ ,  $a = \text{apical}$ ,  $\text{Y} = \text{F}$ ,  $\text{Cl}$ ,  $\text{Br}$ ,  $\text{I}$ ,  $\text{OH}$ ,  $\text{CN}$  ...) located in terminal positions. For illustration, the  $[\text{Mo}_6\text{Br}_8^i\text{Br}_6^a]^{2-}$  cluster unit is represented in Figure 1. These cluster units are associated with inorganic or organic cations in many compounds of general formula  $\text{A}_n[\text{M}_6\text{X}_8^i\text{Y}^a_6]$  ( $\text{A} = \text{alkali cation}$ , quaternary ammonium,  $\text{H}_3\text{O}^+$  ...) prepared either by solid state chemistry

or by combined use of solid state and solution chemistries.  $A_n[M_6X_8Y_6]$  series afford thus useful  $[M_6X_8Y_6]^{n-}$  building blocks with specific physico-chemical properties that can be involved in the preparation of molecular assemblies and nanomaterials (e.g.: dendrimers, liquid crystal and polymer nanocomposites, functional surfaces).<sup>29-39</sup>

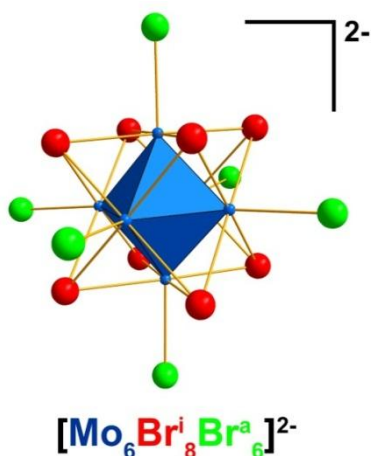


**Figure 1.** Schematic representation of the  $[Mo_6Br_8Br_6]^{2-}$  cluster unit.

The present work focuses on the encapsulation of molybdenum octahedral cluster bromide units, namely  $[Mo_6Br_{14}]^{2-}$ , in silica nanoparticles using  $Cs_2[Mo_6Br_{14}]$  inorganic solid state compound as cluster precursor.  $[Mo_6Br_{14}]^{2-}$  units are about 1 nm in size as reported in previous crystallographic characterizations.<sup>40</sup> Under UV or visible excitation, they exhibit a broad emission from 550 to 900 nm with a maximum around 780 nm.<sup>41</sup> Maverick *et al.* reported a photoluminescence quantum yield of 23% with a lifetime of 130  $\mu s$  for these cluster units in acetonitrile solution at room temperature.<sup>41</sup> However, the photoluminescence of cluster units is easily quenched in aqueous solution owing to the presence of oxygen that form singlet oxygen through a non radiative process involving the cluster.<sup>42</sup> It is worth noting that such reactive oxygen species (ROS) are used as theranostic agent for photodynamic therapy (PDT).<sup>43</sup>

Here is reported an extended study on luminescent  $Cs_2[Mo_6Br_{14}]@SiO_2$  nanoparticles prepared by water-in-oil microemulsion. The nanoparticles were characterized by means of electron microscopy techniques, photoluminescence spectrometry, nuclear magnetic resonance spectroscopy, elemental analysis and nitrogen physisorption. This work bring a better understanding of the physico-chemical properties of these nanoparticles. A particular attention has been be paid to the chemical modifications experienced by the cluster units during the encapsulation process and to their structural interactions with the surrounding silica matrix. The results and discussion constitute therefore an important step toward a better control of their optical properties. Finally, the toxicity of  $Cs_2[Mo_6Br_{14}]@SiO_2$  nanoparticles was evaluated by using

recently developed nanotoxicity tests on plants<sup>44</sup> and by human cell proliferation assays.

## 2. Experimental part

**2.1. Chemicals and cluster precursor.** Polyoxyethylene (4) lauryl ether (Brij®30) and tetraethoxysilane (TEOS, 98.00%) were purchased from Sigma-Aldrich. Ammonia (28 wt% in water) and *n*-heptane (99.00%) were purchased from VWR. Ethanol (99.80%) was purchased from Fluka. The  $Cs_2[Mo_6Br_{14}]$  cluster compound was prepared according to published procedure.<sup>40</sup>

**2.2 Synthesis of the  $Cs_2[Mo_6Br_{14}]@SiO_2$  nanoparticles.** The  $Cs_2[Mo_6Br_{14}]@SiO_2$  nanoparticles were synthesized by a water-in-oil microemulsion process as previously described.<sup>25,26</sup> First, a cluster sol was prepared by dissolving the  $Cs_2[Mo_6Br_{14}]$  cluster compound in a mixture of ethanol and distilled water (1:1 volume ratio). The concentration of the cluster sol could be varied up to 0.02 M. The microemulsion was prepared by mixing 47 ml of *n*-heptane and 15 ml of Brij®30, followed by the dropwise addition of 1.6 ml of the cluster sol and 1.3 ml of an ammonia solution. In order to preserve the stability of the cluster units at all steps, it is important that the cluster compound is first solvated in absolute ethanol and then fully dissolved by addition of the water. For the same reason, this cluster sol has to be added to the heptane and Brij®30 mixture separately from the ammonia solution. Deviations from this procedure or addition of the ammonia solution to the cluster sol outside of the microemulsion would result in a quick precipitation of the cluster units. After 1 hour of magnetic stirring to insure homogeneity of the microemulsion, 2 ml of TEOS were added. The reaction was left under magnetic stirring for 3 days. Then, the microemulsion was destabilized by the addition of ethanol (~ 80 ml). Finally, the nanoparticles were collected and washed by several centrifugation cycles which are summarized in Table 1 before dispersion in purified water.

**Table 1. Summary of the 9 steps centrifugation protocol used for the purification of the  $Cs_2[Mo_6Br_{14}]@SiO_2$  nanoparticles indicating the solvent used in each step, the relative centrifugal force (RCF) and the centrifugation time. Between each step, the nanoparticles were redispersed in solvent by sonication. The steps 3 to 9 are identical.**

step	solvent	RCF (g)	time (min)
1	microemulsion + ethanol	10000	10
2	ethanol	20000	20
3 to 9	water	40000	30

**2.3. Characterization techniques.** The size and morphology of the  $Cs_2[Mo_6Br_{14}]@SiO_2$  nanoparticles were

characterized by field emission scanning electron microscopy (FE-SEM) using a Hitachi SU8000 microscope operating at 10 kV, and by transmission electron microscopy (TEM) using a JEOL JEM-1400 microscope operating at 120 kV. The presence of the cluster units inside the silica nanoparticles was characterized by high angle annular dark field scanning transmission electron microscopy (HAADF-STEM) using a Hitachi High-Technologies HD-2300C microscope operating at 200 kV (full setup details can be found in ref. <sup>27</sup>). The Cs<sub>2</sub>[Mo<sub>6</sub>Br<sub>14</sub>]/SiO<sub>2</sub> nanoparticles were analyzed by inductively coupled plasma optical emission spectrometry (ICP-OES) for dosage of the Si, Cs, Mo and Br elements. The photoluminescence properties were characterized using a Horiba Jobin Yvon Fluorolog-3 spectrophotometer. The nanoparticles were analyzed by solid state <sup>1</sup>H and <sup>29</sup>Si magic-angle-spinning nuclear magnetic resonance (MAS NMR) using a Bruker Ultrashield 300 WB spectrometer. We employed 4 mm and 2.5 mm MAS probes for <sup>29</sup>Si and <sup>1</sup>H MAS NMR respectively. Spectra were recorded with spinning rates of 10 kHz and 30 kHz for <sup>29</sup>Si and <sup>1</sup>H MAS NMR respectively. The chemical shifts were calibrated using a reference of tetramethylsilane (TMS) for <sup>29</sup>Si MAS NMR and distilled water for <sup>1</sup>H MAS NMR. The specific surface area of Cs<sub>2</sub>[Mo<sub>6</sub>Br<sub>14</sub>]/SiO<sub>2</sub> and SiO<sub>2</sub> nanoparticles was measured by the Brunauer-Emmett-Teller method (BET) using a Micromeritics Tristar 3000.

**2.4. Plant culture systems and biomass determination.** Seeds of rapeseed (*Brassica napus*) of the drakkar ecotype have been used. Plant culture system and test procedures were similar to those previously described for the evaluation of the toxicity of the Cs<sub>2</sub>[Mo<sub>6</sub>Br<sub>14</sub>] cluster compound before its encapsulation in silica nanoparticles.<sup>44</sup> Briefly, eight rapeseed seeds were transferred onto sterilized filter papers (Whatman n°3) disposed in 90 mm × 15 mm Petri dishes containing 4 ml of an aqueous solution of Cs<sub>2</sub>[Mo<sub>6</sub>Br<sub>14</sub>]/SiO<sub>2</sub> or SiO<sub>2</sub> nanoparticles at 1000 µg/ml. Controls have been prepared by dispersing pure Milli-Q water. The dishes were then sealed and placed in a phytotron for germination and growth of the plants at 24 °C in the dark for 5 days. Once the seedlings harvested, the fresh shoots and roots were separated and their biomass was immediately measured. Each experiment was conducted four times, i.e. four Petri dishes containing eight seedlings each. The biomass results are presented as mean ± SE (standard error of the mean) of the three independent experiments.

**2.5. Human cell culture and cell proliferation (MTT) assay.** Two cell lines were used: Caco-2 a human colon adenocarcinoma cell line and MRC-5 a human lung fibroblast. The cell lines were obtained from American Tissue Culture Collection (ATCC, Rockville, MD, United States). The cells were passaged twice every week and grown in Dulbecco's modified Eagle's medium (DMEM) supple-

mented with 2 mM L-glutamate, 10% fetal calf serum (FCS), 1 mg/L streptomycin, and 1000 U/L penicillin (Complete DMEM). Cells were cultured at 37 °C, 5% CO<sub>2</sub>, and 90% relative humidity. Cell proliferation was determined using the MTT (methylthiazolyl diphenyl tetrazolium bromide) method. Caco-2 and MRC-5 cells were plated in 96-well plates at densities of 3×10<sup>3</sup> cells/well and 6×10<sup>3</sup> cells/well respectively, and with 100 µl of culture medium (10% FBS) per well. After incubating overnight to allow cell attachment, the cells were treated with nanoparticles solutions ranging from 0.1 to 100 µg/ml for 24 hours and 72 hours, and 20% of MTT (5 mg/ml in PBS 1X) reagent was then added for 4 h. The medium was removed, 100 µl of DMSO was added to the cells for 5 min and they were gently shaken. Absorbance at 570 nm was measured using a Micro Plate Reader. Control was cell lines without nanoparticles and the results were expressed in function of this control (=100%). The experiments were performed with these cell monolayers in triplicate.

### 3. Results

**3.1. Size and morphology.** After purification according to the optimized procedure summarized in Table 1, it turns out that no trace of surfactant (Brij<sup>®</sup>30) remains on the nanoparticles as evidenced by <sup>1</sup>H MAS NMR (see Supporting Information, Figure S1). Indeed, after dispersing the nanoparticles in distilled water, the aqueous Cs<sub>2</sub>[Mo<sub>6</sub>Br<sub>14</sub>]/SiO<sub>2</sub> colloid appeared clear without visible light scattering (Figure 2). The size and morphology of the nanoparticles were characterized by FE-SEM and TEM (Figure 3). The electron microscopy images show that the nanoparticles are perfectly spherical and monodisperse in size, with an average diameter of 45 nm. Experiments showed that the concentration of the cluster sol did not affect the size of the nanoparticles in the studied range (up to 0.02 M). The presence of the clusters inside the silica nanoparticles can be evidenced by HAADF-STEM, as previously demonstrated.<sup>25,26</sup> The Figure 4 shows a Z-contrast image of a the Cs<sub>2</sub>[Mo<sub>6</sub>Br<sub>14</sub>]/SiO<sub>2</sub> nanoparticles obtained with this technique, where the cluster units appear as bright spots of about 1 nm in size and homogeneously distributed in the silica matrix.



**Figure 2.** Photography of a Cs<sub>2</sub>[Mo<sub>6</sub>Br<sub>14</sub>]@SiO<sub>2</sub> colloid in water (mass concentration ~ 10 g/L).

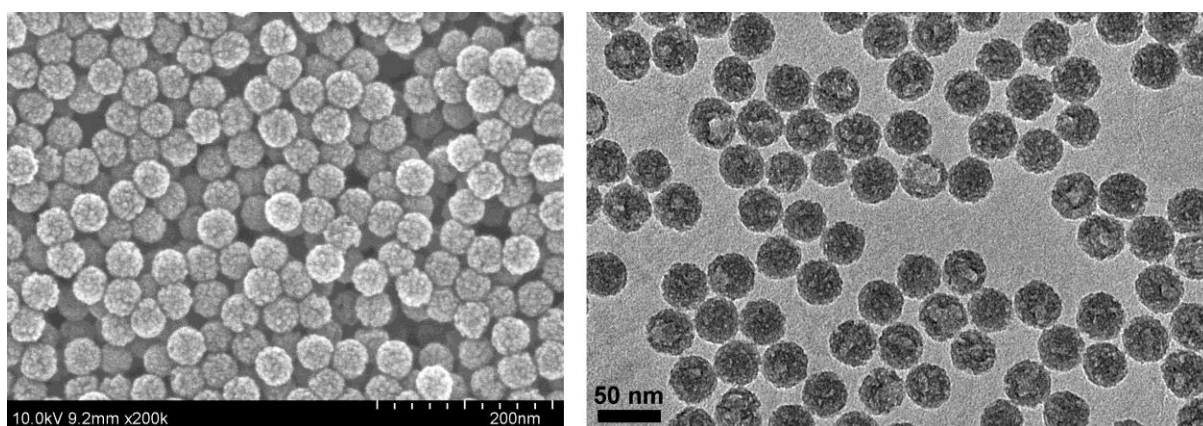


**Figure 3.** FE-SEM image (left) and TEM image (right) of Cs<sub>2</sub>[Mo<sub>6</sub>Br<sub>14</sub>]@SiO<sub>2</sub> nanoparticles.

Regarding the morphology of the Cs<sub>2</sub>[Mo<sub>6</sub>Br<sub>14</sub>]@SiO<sub>2</sub> nanoparticles, the TEM image (Figure 3) suggests a high porosity of the silica matrix which does not appear homogeneous. Indeed, the specific surface area obtained by BET measurements is  $347.7 \pm 9.5 \text{ m}^2/\text{g}$  to be compared with the theoretical value roughly equal to  $60 \text{ m}^2/\text{g}$  for a perfectly smooth sphere of 45 nm in diameter and considering a density of 2.2 for the silica. On the other hand, the specific surface area obtained by BET measurements of bare SiO<sub>2</sub> nanoparticles prepared in the same conditions as the Cs<sub>2</sub>[Mo<sub>6</sub>Br<sub>14</sub>]@SiO<sub>2</sub> nanoparticles is  $327.6 \pm 12.6 \text{ m}^2/\text{g}$  which is roughly equal to the  $347.7 \pm 9.5 \text{ m}^2/\text{g}$  given the error. It can be concluded that the experimental high specific surface area of the nanoparticles results from the synthesis process and not from the encapsulation of the cluster units.

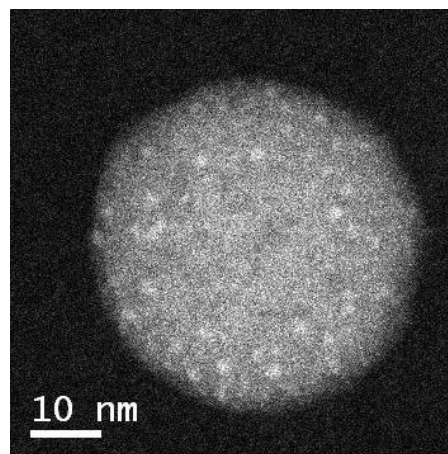


**Figure 4.** HAADF-STEM image of a Cs<sub>2</sub>[Mo<sub>6</sub>Br<sub>14</sub>]@SiO<sub>2</sub> nanoparticle.

**3.2. Chemical composition.** The concentration of cluster units inside the silica nanoparticles was determined with ICP-OES analyses by dosing the Si, Cs, Mo and Br elements. Cs<sub>2</sub>[Mo<sub>6</sub>Br<sub>14</sub>]@SiO<sub>2</sub> nanoparticles prepared with

different concentration of the cluster sol were analyzed. The results are plotted in Figure 5 as molar ratio between Si and the elements of the cluster compound (Cs, Mo and Br). The experimental results are also compared with the theoretical ratio that were calculated assuming that all the TEOS has condensed to form silica and that all the introduced cluster compound is encapsulated in the silica nanoparticles. It appears that the concentration of clusters inside the silica nanoparticles evolves linearly with the concentration of the cluster sol. However, the results show that the experimental concentration of clusters is always below the theoretical one and that the deviation is increasing as the concentration of the cluster sol increases. This observation indicates that the efficiency of the encapsulation of the clusters inside the silica nanoparticles is decreasing when increasing the amount of clusters involved in the synthesis. The results in Figure 5 also show that the deviation between the theoretical and experimental data is more important in the case of Br than for the other elements. Indeed, the results indicate an average  $[\text{Mo}]/[\text{Br}]$  ratio of 0.73 and an average  $[\text{Mo}]/[\text{Cs}]$  ratio of 7.0, whereas the theoretical ones are 0.43 and 3 respectively. Considering the strong stability of the  $\text{Mo}_6$  cluster, these differences can only be explained by the departure of Br and Cs atoms during the encapsulation process. Considering 6 atoms of the  $\text{Mo}_6$  cluster, these ratios give an equivalent of 8.2 atoms of Br and 0.9 atom of Cs per  $\text{Mo}_6$  clusters. The value of 8.3 Br per  $\text{Mo}_6$  cluster corresponds to chemical composition of the  $\text{Mo}_6\text{Br}_8^i$  cluster core characterized by strong Mo-Mo and Mo- $\text{Br}^i$  covalent bonds. This clearly indicates that apical ligands are removed during the encapsulation process. Apical Br ligands are known to be much more labile than the inner  $\text{Br}^i$  ligands owing to more ionic and weak Mo- $\text{Br}^a$  bonds compared to Mo- $\text{Br}^i$ . Two hypotheses can explain the loss of one cesium cation in the nanoparticles compared to the two cesium cations in  $\text{Cs}_2[\text{Mo}_6\text{Br}_{14}]$ . The first one is the oxidation of the cluster units from  $[\text{Mo}_6\text{Br}_{14}]^{2-}$  to  $[\text{Mo}_6\text{Br}_8\text{L}^a_6]^-$  but in this case the photoluminescence properties should be lost. The second one, which is more plausible, could be a partial cationic metathesis involving the replacement of  $\text{Cs}^+$  by  $\text{NH}_4^+$  ions present due to the use of ammonia in the process.

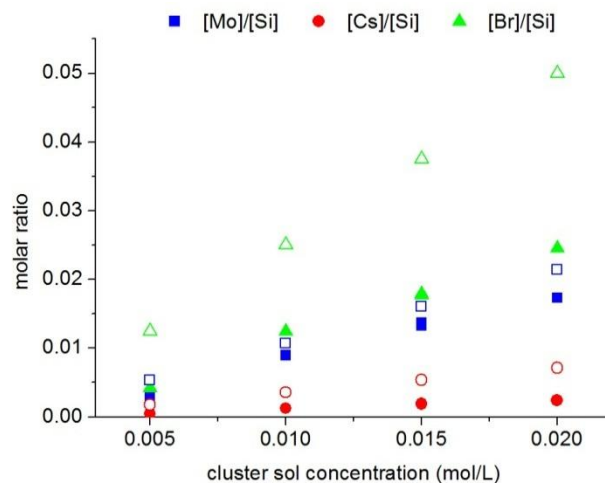


**Figure 5.** Molar ratios between Si and the elements of the cluster compound measured by ICP-OES (full symbols) and theoretically calculated (empty symbols), depending on the concentration of the cluster sol used for the synthesis of the  $\text{Cs}_2[\text{Mo}_6\text{Br}_{14}]\text{@SiO}_2$  nanoparticles.

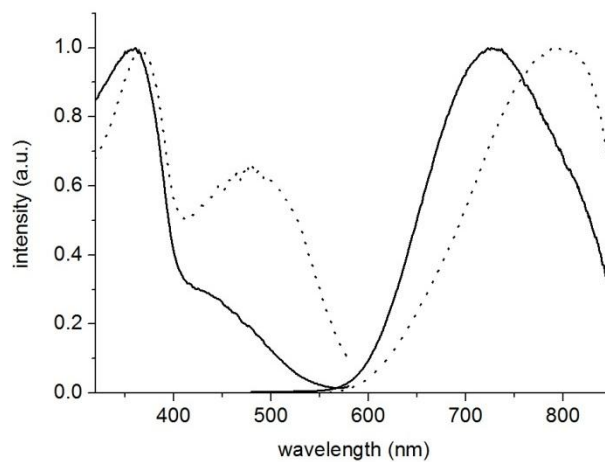


**Figure 6.** Emission and excitation spectra of the  $\text{Cs}_2[\text{Mo}_6\text{Br}_{14}]$  cluster compound (dashed lines) and the  $\text{Cs}_2[\text{Mo}_6\text{Br}_{14}]\text{@SiO}_2$  nanoparticles (continuous line). The emission spectra were recorded for an excitation wavelength of 450 nm and the excitation spectra were recorded at the maximums of emission. The spectra are normalized and the signals are corrected regarding the sensitivity of the detector (photomultiplier).

**3.3. Luminescence properties.** The luminescence properties of the  $\text{Cs}_2[\text{Mo}_6\text{Br}_{14}]\text{@SiO}_2$  nanoparticles were investigated on solid state (powder) and compared to those of the starting  $\text{Cs}_2[\text{Mo}_6\text{Br}_{14}]$  cluster compound. The obtained emission and excitation spectra are gathered in Figure 6. They show that the encapsulation of the clusters results in a shift of the emission maximum of roughly 70 nm to lower wavelengths. A similar shift in the emission wavelength has been reported for the encapsulation of the  $\text{Cs}_4[\text{Re}_6\text{S}_8\text{Br}_6]$  cluster compound.<sup>27</sup> In this case, the emission spectrum of  $\text{Cs}_4[\text{Re}_6\text{S}_8\text{Br}_6]\text{@SiO}_2$  nanoparticles appeared to be very similar to that of  $\text{K}_4[\text{Re}_6\text{S}_8(\text{OH})_6]\text{@SiO}_2$

nanoparticles. Thus, it was suggested that the apical Br ligands could be exchanged for OH groups during the encapsulation process, provoking the emission shift. However, in the case of Mo<sub>6</sub> clusters, the [Mo<sub>6</sub>Br<sub>8</sub>(OH)<sub>6</sub>]<sup>2-</sup> cluster unit has not yet been isolated to check whether the Cs<sub>2</sub>[Mo<sub>6</sub>Br<sub>14</sub>]@SiO<sub>2</sub> nanoparticles would have the same emission properties.

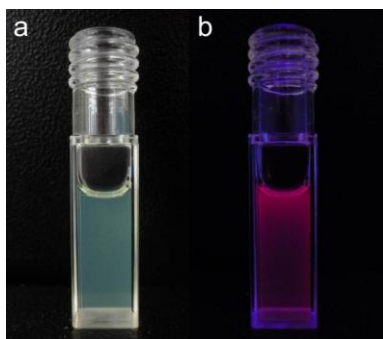


**Figure 7.** Photographs of a Cs<sub>2</sub>[Mo<sub>6</sub>Br<sub>14</sub>]@SiO<sub>2</sub> colloid in water under day light (a) and under UV excitation at 365 nm (b).

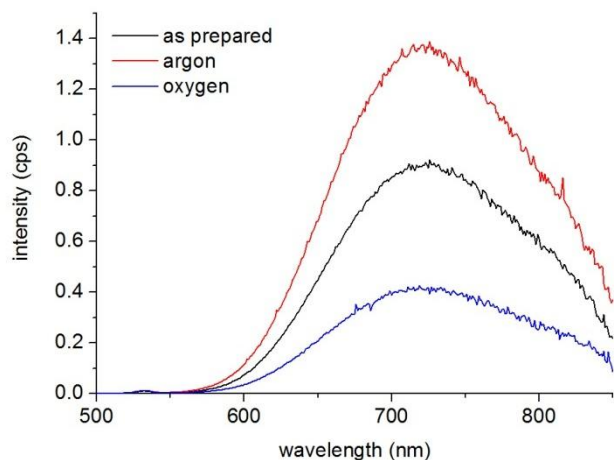


**Figure 8.** Emission spectra of a Cs<sub>2</sub>[Mo<sub>6</sub>Br<sub>14</sub>]@SiO<sub>2</sub> colloid in water: as prepared, and after argon or oxygen bubbling. The emission spectra were recorded for an excitation wavelength of 450 nm and the signals were corrected regarding the sensitivity of the detector (photomultiplier).

An important feature of these nanoparticles is that the silica matrix protect the cluster units from the presence of oxygen in aqueous solution. Indeed, the cluster@SiO<sub>2</sub> nanoparticles remain luminescent even in water as illustrated in Figure 7. The efficiency of the protective effect of the silica against oxygen was carefully investigated on a Cs<sub>2</sub>[Mo<sub>6</sub>Br<sub>14</sub>]@SiO<sub>2</sub> colloid in water using photoluminescence spectrometry (Figure 8). The emission spectrum of a Cs<sub>2</sub>[Mo<sub>6</sub>Br<sub>14</sub>]@SiO<sub>2</sub> colloid was recorded after synthesis and purification of the nanoparticles. The dissolved oxygen in solution was completely removed by bubbling argon through the colloid for 3 hours. The emission spectrum of the colloid was recorded again showing

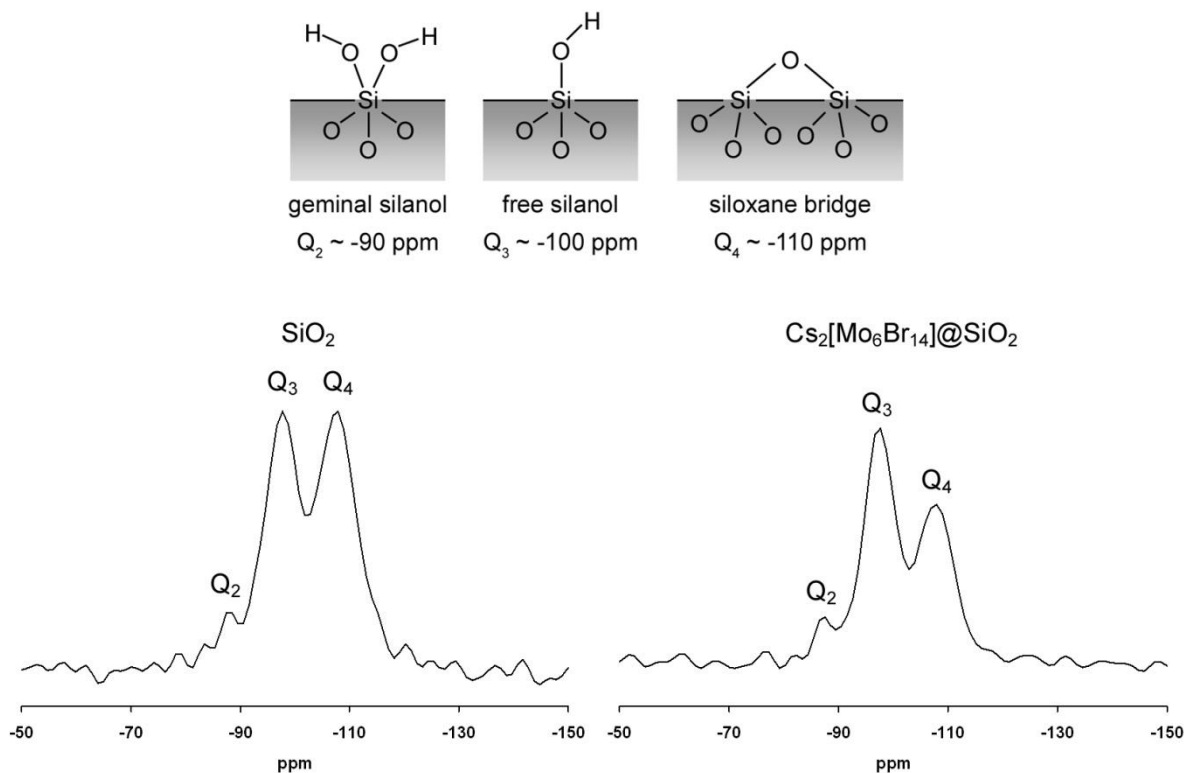


**Figure 9.** Top: illustration of the  $Q_2$ ,  $Q_3$  and  $Q_4$  silicon atoms with their respective chemical shift. Bottom:  $^{29}\text{Si}$  MAS NMR spectra of  $\text{SiO}_2$  (left) and  $\text{Cs}_2[\text{Mo}_6\text{Br}_{14}]\text{@SiO}_2$  (right) nanoparticles.

an increase in the luminescence intensity. Then, the solution was saturated again with oxygen by bubbling oxygen for 5 minutes, what resulted in a decrease of about 70% of the emission intensity. Longer oxygen bubbling (up to 24 hours) did not provoke any further decrease of the emission intensity. Thus, the efficiency of the protection of the silica matrix is not absolute. Due to the porosity of the nanoparticles, dissolved oxygen still have access to their inner part and therefore to the cluster units. However, it also appeared that a part of the cluster units are definitively protected because an extended exposition to oxygen (24h) did not resulted in a complete quenching of the luminescence. This is most likely due to cluster units located in parts of the silica matrix where oxygen does not diffuse. Thanks to these two findings, these nanoparticles have a great potential for both fluorescence imaging and PDT applications. To remove oxygen quenching another possible solution could be to grow post-synthesis an additional shell of silica around the nanoparticles through a seeded process.<sup>7</sup>

**3.4. Microstructural properties.** In order to study the influence of the cluster units on the microstructural properties of the silica,  $\text{Cs}_2[\text{Mo}_6\text{Br}_{14}]\text{@SiO}_2$  nanoparticles were analyzed by  $^{29}\text{Si}$  MAS NMR and compared to bare  $\text{SiO}_2$  nanoparticles prepared in the same conditions. The spectra of both samples (Figure 9) show three signals at

chemical shifts of  $\delta = -90$  ppm,  $\delta = -100$  ppm and  $\delta = -110$  ppm, respectively assigned to  $Q_2$  geminal silanols,  $Q_3$  free silanols, and  $Q_4$  siloxane bridges (see Figure 9).<sup>45</sup> The integrated areas calculated after deconvolution of the three signals indicated a decrease of 20% of the proportion in  $Q_4$  silicon in  $\text{Cs}_2[\text{Mo}_6\text{Br}_{14}]\text{@SiO}_2$  nanoparticles compared to  $\text{SiO}_2$  nanoparticles. However, this decreased can also be interpreted as an increase of the silanols in the silica matrix. The influence of the cluster units on the siloxanes over silanols ratios is probably a result of their interaction with the silica matrix and will be developed in the discussion section.

**3.5. Phytotoxicity tests.** We recently reported that  $\text{Cs}_2[\text{Mo}_6\text{Br}_{14}]$  cluster compound can have toxic effects on plants.<sup>44</sup> In order to investigate the effects of the encapsulation of cluster units on their toxicity, the phytotoxicity of  $\text{Cs}_2[\text{Mo}_6\text{Br}_{14}]\text{@SiO}_2$  nanoparticles was studied. The same tests were also performed on  $\text{SiO}_2$  nanoparticles without cluster to determine if potential toxic effects come from the clusters or the silica nanoparticles themselves. Plants were treated with  $\text{SiO}_2$  and  $\text{Cs}_2[\text{Mo}_6\text{Br}_{14}]\text{@SiO}_2$  nanoparticles in water at 1000  $\mu\text{g}/\text{ml}$ . In the case of the  $\text{Cs}_2[\text{Mo}_6\text{Br}_{14}]\text{@SiO}_2$  nanoparticles, it amounts to an embedded Mo concentration of 0.23 mM as determined by ICP-OES analysis. It was showed previously that this dose of 0.23 mM of Mo is sufficient to

cause growth inhibition when the source of Mo is  $\text{Cs}_2[\text{Mo}_6\text{Br}_{14}]$  cluster compound.<sup>44</sup> It appears in the present work that neither  $\text{SiO}_2$  nanoparticles nor  $\text{Cs}_2[\text{Mo}_6\text{Br}_{14}]\text{@SiO}_2$  nanoparticles have any significant effect on the plants growth. Values of plant root and aerial part biomass after 5 days of growth in the dark are shown in Figure 10. In addition, the nanoparticles did not affect the morphology of the plants as it was the case with  $\text{Cs}_2[\text{Mo}_6\text{Br}_{14}]$  cluster compound.<sup>44</sup> The root surface of  $\text{SiO}_2$  and  $\text{Cs}_2[\text{Mo}_6\text{Br}_{14}]\text{@SiO}_2$  treated plants were in intimate contact with the nanoparticles but did not show any abnormal appearance as observed with FE-SEM (see Supporting Information, Figure S9).

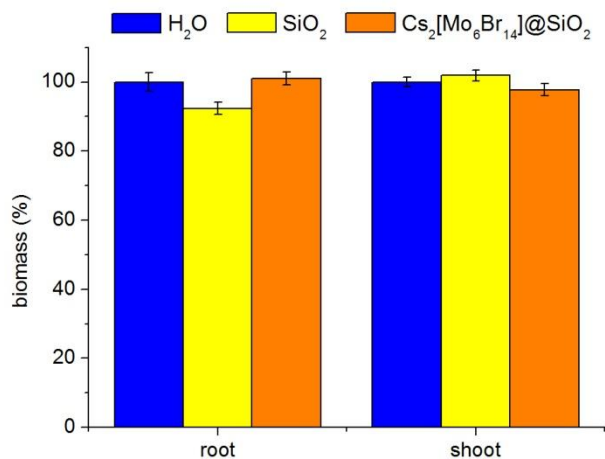


**Figure 10.** Root and shoot biomass of plants treated with  $\text{SiO}_2$  or  $\text{Cs}_2[\text{Mo}_6\text{Br}_{14}]\text{@SiO}_2$  nanoparticles in water at 1000  $\mu\text{g/ml}$ , and compared with negative controls ( $\text{H}_2\text{O}$ ). All root and shoot growth data are expressed as percentages of root or shoot growth in  $\text{H}_2\text{O}$  negative control.

**3.6. Human cell proliferation.** The cytotoxicity of  $\text{Cs}_2[\text{Mo}_6\text{Br}_{14}]\text{@SiO}_2$  nanoparticles was also investigated for the first time on two different cell lines. The results of cell viability depending on the nanoparticles concentration and incubation time are reported in Figure 11. For epithelial gut cell Caco-2, after 24h of contact with the nanoparticles, no variation in the cell proliferation could be observed for concentrations between 0.1 and 10  $\mu\text{g/ml}$ . In these cases, the human cell viability was always higher than 91% of the control test without nanoparticle. For concentrations between 25 and 100  $\mu\text{g/ml}$ , the cell toxicity was slightly increased, but the cell viability remained at least higher than 80% of the control. After 72h contact, the proliferation of the Caco-2 cell was comparable to the results obtained for 24h of contact. The lowest cell viability (85%) was observed in the case a nanoparticles concentration of 100  $\mu\text{g/ml}$ .

For human fibroblast MRC-5, after 24h of contact the cell proliferation was relatively reduced compared to the Caco-2 cell line but remained above 80% of the control

for concentrations up to 10  $\mu\text{g/ml}$ . For concentrations of 25 and 50  $\mu\text{g/ml}$ , the cytotoxicity of the nanoparticles was moderate, with 73 and 75% respectively. For the highest tested concentration of 100  $\mu\text{g/ml}$ , the cytotoxic effects were important with only 59% of cell viability compared to the control. After 72h of incubation with the nanoparticles, the fibroblast proliferation showed comparable results as for 24h of contact with significantly increased toxicity for nanoparticles concentrations higher than 25  $\mu\text{g/ml}$ .

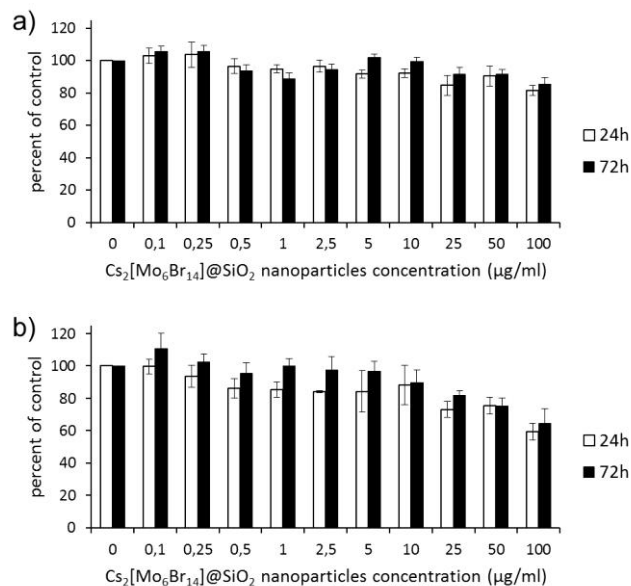


**Figure 11.** Viability of Caco-2 (a) and MRC-5 (b) human cells depending on the concentration of  $\text{Cs}_2[\text{Mo}_6\text{Br}_{14}]\text{@SiO}_2$  nanoparticles and for two different incubation times.

#### 4. Discussion

We showed that  $[\text{Mo}_6\text{Br}_{14}]^{2-}$  cluster units can be easily encapsulated in silica nanoparticles by a water-in-oil microemulsion process without any modification of their morphology, meaning the size, monodispersity and specific surface area of the synthesized silica nanoparticles. As previously reported,<sup>4</sup> the preparation of  $\text{Cs}_2[\text{Mo}_6\text{Br}_{14}]\text{@SiO}_2$  nanoparticles by a Stöber process is also possible but in this case the size of the synthesized nanoparticles strongly depends on the cluster concentration (see Supporting Information, paragraph 2.). The  $\text{Cs}_2[\text{Mo}_6\text{Br}_{14}]\text{@SiO}_2$  nanoparticles reported here are particularly stable as the cluster units do not leak from the nanoparticles, even after repeated centrifuging cycles at relatively high relative centrifugal force (up to 40000 g) in ethanol or in water (see Supporting Information, Figure S3).

These observations suggest a strong interaction between the cluster units and the silica matrix. Gao *et al.* failed in incorporating negatively charged and charge-neutral  $\text{Re}_6$  based cluster units in silica nanoparticles,<sup>43</sup> which is contrary to what we report here for  $\text{Mo}_6$  based

cluster units and previously reported for  $\text{Re}_6$  based cluster units.<sup>27</sup> However, they succeeded in incorporating positively charged  $\text{Re}_6$  cluster units and therefore claimed an electrostatic interaction. Here, the hypothesis of an electrostatic interaction can be excluded as both the encapsulated cluster units and the silica matrix are negatively charged in our synthesis conditions. Thus, two hypotheses should be considered: hydrogen bonds or covalent bonds, which are schematically illustrated in Figure 12.

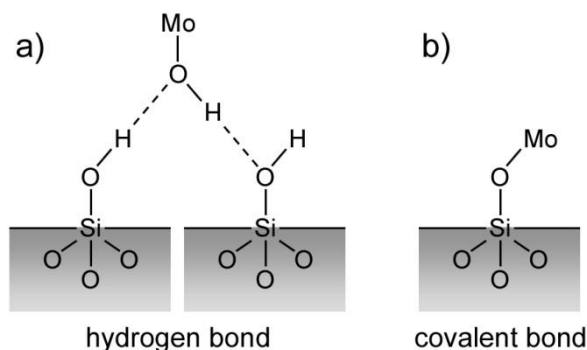


**Figure 12.** Schematic illustration of the possible types of interaction between the clusters units and the silica matrix. (a) In the hypothesis where the apical Br ligands are exchanged for OH groups during the microemulsion process, the cluster units can interact with the silanols of the silica matrix through the formation of hydrogen bonds. (b) In the hypothesis where the apical Br ligands are eliminated during a condensation process, the cluster units can covalently bond to the silica.

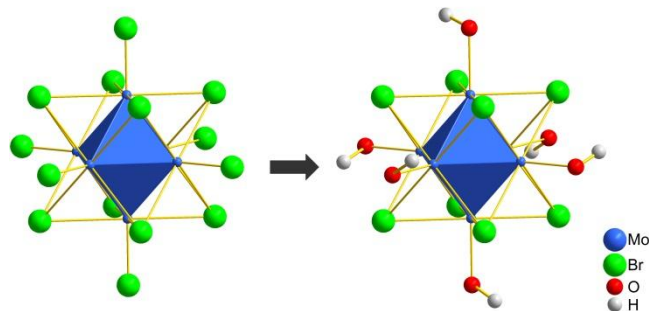
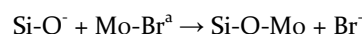


**Figure 13.** Schematic illustration of the possible ligand exchange experienced by the cluster units, from  $[\text{Mo}_6\text{Br}_8\text{Br}^a_6]^{2-}$  (left) to  $[\text{Mo}_6\text{Br}_3(\text{OH})^a_3]^{2-}$  (right).

We showed by ICP-OES analysis that the apical Br ligands of the cluster units are eliminated during the encapsulation process. As schematically illustrated in Figure 13, these ligands can be exchanged for OH groups as a result of the hydrolysis of the cluster compound.<sup>46</sup> This OH groups at the apical positions of the cluster units would therefore readily create hydrogen bonds with the silanol groups of the silica nanoparticles under formation. This exchange would be consistent with the optical properties of the  $\text{Cs}_2[\text{Mo}_6\text{Br}_{14}]\text{@SiO}_2$  nanoparticles which showed a shift of the maximum of emission of the cluster units. This exchange could also be observed by UV-visible spec-

troscopy as  $\text{Cs}_2[\text{Mo}_6\text{Br}_{14}]\text{@SiO}_2$  nanoparticles show the same absorption spectrum as hydrolyzed cluster units after 5 days in water and differ from the non-hydrolyzed cluster units in ethanol (see Supporting Information, Figure S4). The  $^{29}\text{Si}$  MAS NMR results, i.e. the differences in the ratio between siloxanes and silanols, indicate that  $\text{Cs}_2[\text{Mo}_6\text{Br}_{14}]\text{@SiO}_2$  nanoparticles show a higher content of silanol groups than bare silica nanoparticles. This could be consistent with an interaction through hydrogen bonds between OH groups in the apical positions of the cluster units and the silanol groups of the hydrolyzed silica monomers or of the silica nanoparticles under formation. Indeed, these silanols occupied by cluster units are no longer able to condense to form siloxane bridges as if they were forming hydrogen bonds with water molecules. As a result, the formation of such hydrogen bonds leads to silica nanoparticles with a higher content of silanol groups. On the other hand, the hydrolysis of the cluster units should result in their aggregation whereas HAADF-STEM images (Figure 4) showed that they are isolated and well dispersed in the silica matrix.

Regarding the hypothesis of the formation of covalent bonds between the cluster units and the silica matrix, the apical Br ligands can also be eliminated through the condensation of the cluster units with silanol groups of the silica matrix under formation, according to the following base-catalyzed nucleophilic substitution reaction:



Thus, in this hypothesis the apical Br ligands are not replaced by OH groups anymore but by “OSi” groups. This modification of the cluster units can also explain the optical properties of the  $\text{Cs}_2[\text{Mo}_6\text{Br}_{14}]\text{@SiO}_2$  nanoparticles. Indeed, the exchange for OH or OSi groups may have a similar influence on the molecular orbital diagram of the cluster units. Robinson *et al.* reported that such covalent bonding was possible for cluster units with a  $\text{Mo}_6\text{Cl}_8$  core when apical ligands are labile,<sup>47</sup> which is the case of the Br apical ligands. However, we could not identify the presence of Si-O-Mo bonds by Raman or infrared spectroscopy. It was actually already suggested by Robinson *et al.* that these techniques would not be sensitive enough to evidence such bonds in a similar system due to the important background signals of  $\text{SiO}_2$  and to the breadth of the UV-visible and luminescence spectra of the cluster units.<sup>47</sup> We can reasonably estimate that the cluster units interact with the silica matrix through both hydrogen bonds and covalent bonds, the apical Br ligands being partially exchanged by OH groups and partially by OSi groups. Taking also into account the partial cationic metathesis involving the replacement of  $\text{Cs}^+$  by  $\text{NH}_4^+$  as evidenced by ICP-OES, the cluster compound inside the silica nanoparticles should therefore have the following

formula:  $(\text{Cs}, \text{NH}_4)[\text{Mo}_6\text{Br}_8(\text{OSi})^a_{6-x}(\text{OH})^a_x]$ , with  $x$  comprised between 0 and 6.

From the beginning of the design of luminescent silica nanoparticles, we were very concerned about their potential toxic impact. Regarding phytotoxicity, in contrast to what was observed for individual cluster units,<sup>44</sup> it appeared that the  $\text{Cs}_2[\text{Mo}_6\text{Br}_{14}]\text{@SiO}_2$  nanoparticles have no effect on plant growth (Figure 10) or morphology (see Supporting Information, Figure S9) in dark conditions. As a matter of fact, the silica encapsulation of the clusters protects the plant cells by avoiding direct contact of harmful clusters with cellular structures. However, as already mentioned excited cluster units can relax non-radiatively through the formation of singlet oxygen, which is of toxicological concern as these species can provoke an oxidative stress and damages on plant tissues.<sup>48</sup> In this sense, it is worth to be noted that for additional experiments with plant growth under a 16h light ( $115 \mu\text{mol}/\text{m}^2/\text{s}$ ) period per day, the  $\text{Cs}_2[\text{Mo}_6\text{Br}_{14}]\text{@SiO}_2$  nanoparticles did not show any significant toxic effect either (data not shown). Indeed, we showed that once encapsulated in silica the cluster units remain luminescent even when the nanoparticles are dispersed in water, thus indicating that oxygen cannot access the clusters anymore limiting therefore the formation of singlet oxygen.

Regarding the toxicity on human cells, our study showed that the toxicity of the  $\text{Cs}_2[\text{Mo}_6\text{Br}_{14}]\text{@SiO}_2$  nanoparticles is lower with Caco-2 epithelial cells than with lung fibroblasts MRC-5. However, for concentrations between 0.1 and 50  $\mu\text{g}/\text{ml}$ , the decrease in proliferation was very moderate for both cell lines. Cell toxicity became significant only for the fibroblastic cells and for the highest concentration (100  $\mu\text{g}/\text{ml}$ ). The lethal concentration 50 (LC50) for the lung cells Caco-2 and the LC20 for the colon cells MRC-5 are out of the range of studied concentrations (>100 $\mu\text{g}/\text{ml}$ ). In addition, we found no effect of the incubation time on these results. With cell line MRC-5 and with some incubation times, hematite nanoparticles generated a drastic lipid peroxidation increase conversely with a decrease of reduced glutathione concentration which represent a cellular antioxydative system.<sup>49</sup> McCarthy *et al.* reported a strong toxicity for 10 nm sized amorphous silica nanoparticles on human lung submucosal cells with a LC50 of 9.7  $\mu\text{g}/\text{ml}$  after 24h of incubation.<sup>50</sup> With MTT analyses of lung cells A549 and endothelial cells, Lison *et al.* found for 30 nm sized amorphous silica nanoparticles a LC50 of 50  $\mu\text{g}/\text{ml}$  and 100  $\mu\text{g}/\text{ml}$  respectively.<sup>51</sup> Thus, our preliminary results should be pursued by the comparison of the toxicity for the  $\text{Cs}_2[\text{Mo}_6\text{Br}_{14}]\text{@SiO}_2$  nanoparticles with related nanoparticles. Nanomaterials can show multiple properties such as size, shape, specific surface area, degree of aggregation, remaining reaction products, etc. that can vary from a synthesis to another one. For instance, amorphous silica nanoparticles with same size can show different specific surface area because of different porosity/density.

## 5. Conclusions

In conclusion, we reported here an extended study of  $\text{Cs}_2[\text{Mo}_6\text{Br}_{14}]\text{@SiO}_2$  nanoparticles prepared by a water-in-oil microemulsion process. The cluster units were efficiently encapsulated in the silica nanoparticles with a good stability, and the concentration of cluster units could be adjusted without affecting the size and morphology of the silica nanoparticles. We also showed that during the encapsulation process, the cluster units are chemically modified as they lose their apical Br ligands and roughly half of their  $\text{Cs}^+$  counter cations. This loss of ligands resulted in a slight modification of the optical properties of the  $\text{Cs}_2[\text{Mo}_6\text{Br}_{14}]\text{@SiO}_2$  nanoparticles with in particular a blue shift of the maximum of emission. These ligands are most likely exchanged partially by OH groups that can form hydrogen bonds with the silanol groups of the silica and by OSi groups through a covalent bonding between the cluster units and the silica matrix, leading to a cluster compound with the following formula:  $(\text{Cs}, \text{NH}_4)[\text{Mo}_6\text{Br}_8(\text{OSi})^a_{6-x}(\text{OH})^a_x]$ , with  $x$  comprised between 0 and 6. An important feature of these nanoparticles is that the silica matrix protects, to some extent, the cluster units from the presence of oxygen in solution and the nanoparticles remain luminescent even when dispersed in water. In spite of the lack of systematic protocols for the study of the toxicity of nanomaterials, our results indicate that  $\text{Cs}_2[\text{Mo}_6\text{Br}_{14}]\text{@SiO}_2$  nanoparticles do not show any significant toxic effect on the growth and morphology of plants. Regarding cytotoxicity of  $\text{Cs}_2[\text{Mo}_6\text{Br}_{14}]\text{@SiO}_2$  nanoparticles, we observed a dose effect but no time effect. These results should be compared with related silica nanoparticles.

## ACKNOWLEDGMENT

This work was supported by the University of Rennes 1, CNRS, ANR (Project CLUSTOP 2011 BSo8 013 01), Region Bretagne and the College Doctoral Franco-Japonais. Christiane Perrin is acknowledged for helpful discussions. T.A. thanks the 'College Doctoral Franco-Japonais' for attribution of a grant for research at the NIMS. The authors thank Kotone Hasegawa (NIMS) and Joseph Le Lannic (University of Rennes 1) for supplying the SEM images, Agnès Burel (University of Rennes 1) for supplying the TEM images, Yann Le Gal (University of Rennes 1) for the ICP measurements and Laurent Le Gendre (IUT Saint-Brieuc) for the BET measurements.

## ASSOCIATED CONTENT

**Supporting Information:** additional characterizations for  $\text{Cs}_2[\text{Mo}_6\text{Br}_{14}]\text{@SiO}_2$  nanoparticles prepared by water-in-oil microemulsion (<sup>1</sup>H MAS NMR, ICP-OES, UV-visible absorption spectrophotometry); characterizations of  $\text{Cs}_2[\text{Mo}_6\text{Br}_{14}]\text{@SiO}_2$  particles synthesized by a Stöber process; additional characterization on the effect of  $\text{Cs}_2[\text{Mo}_6\text{Br}_{14}]\text{@SiO}_2$  nanoparticles on the growth of plants.

## AUTHOR INFORMATION

### Corresponding Author

\*E-mails: [tangi.aubert@ugent.be](mailto:tangi.aubert@ugent.be) (TA), [fabien.grasset@univ-rennes1.fr](mailto:fabien.grasset@univ-rennes1.fr) (FG), [stephane.cordier@univ-rennes1.fr](mailto:stephane.cordier@univ-rennes1.fr) (SC).

### Present Addresses

ε Ghent University, Department of Inorganic and Physical Chemistry, Physics and Chemistry of Nanostructures group, Krijgslaan 281-S3, 9000 Gent, Belgium.

### Author Contributions

The manuscript was written through contributions of all authors. All authors have given approval to the final version of the manuscript.

### Notes

The authors declare no competing financial interest.

## REFERENCES

- (1) Burns, A.; Vider, J.; Ow, H.; Herz, E.; Penate-Medina, O.; Baumgart, M.; Larson, S. M.; Wiesner, U.; Bradbury, M. Fluorescent Silica Nanoparticles with Efficient Urinary Excretion for Nanomedicine. *Nano Lett.* **2009**, *9*, 442-448.
- (2) Vivero-Escoto, J. L.; Huxford-Phillips, R. C.; Lin, W. Silica-Based Nanoprobes for Biomedical Imaging and Theranostic Applications. *Chem. Soc. Rev.* **2012**, *41*, 2673-2685.
- (3) Noginov, M. A.; Zhu, G.; Belgrave, A. M.; Bakker, R.; Shalae, V. M.; Narimanov, E. E.; Stout, S.; Herz, E.; Suteewong, T.; Wiesner, U. Demonstration of a Spaser-Based Nanolaser. *Nature* **2009**, *460*, 1110-1112.
- (4) Dechézelles, J.-F.; Aubert, T.; Grasset, F.; Cordier, S.; Barthou, C.; Schwob, C.; Maitre, A.; Vallée, R. A. L.; Cramail, H.; Ravaine, S. Fine Tuning of Emission Through the Engineering of Colloidal Crystals. *Phys. Chem. Chem. Phys.* **2010**, *12*, 11993-11999.
- (5) Giesche, H.; Matijevic, E. Well-Defined Pigments: I. Monodispersed Silica-Acid Dyes Systems. *Dyes Pig.* **1991**, *17*, 323-340.
- (6) van Blaaderen, A.; Vrij, A. Synthesis and Characterization of Colloidal Dispersions of Fluorescent, Monodisperse Silica Spheres. *Langmuir* **1992**, *8*, 2921-2931.
- (7) Ow, H.; Larson, D. R.; Srivastava, M.; Baird, B. A.; Webb, W. W.; Wiesner, U. Bright and Stable Core-Shell Fluorescent Silica Nanoparticles. *Nano Lett.* **2005**, *5*, 113-117.
- (8) Santra, S.; Dutta, D.; Moudgil, B. M. Functional Dye-Doped Silica Nanoparticles for Bioimaging, Diagnostics and Therapeutics. *Food Bioprod. Process.* **2005**, *83*, 136-140.
- (9) Chang, S.-Y.; Liu, L.; Asher, S. A. Preparation and Properties of Tailored Morphology, Monodisperse Colloidal Silica-Cadmium Sulfide Nanocomposites. *J. Am. Chem. Soc.* **1994**, *116*, 6739-6744.
- (10) Mulvaney, P.; Liz-Marzan, L. M.; Giersig, M.; Ung, T. Silica Encapsulation of Quantum Dots and Metal Clusters. *J. Mater. Chem.* **2000**, *10*, 1259-1270.
- (11) Gerion, D.; Pinaud, F.; Williams, S. C.; Parak, W. J.; Zanchet, D.; Weiss, S.; Alivisatos, A. P. Synthesis and Properties of Biocompatible Water-Soluble Silica-Coated CdSe/ZnS Semiconductor Quantum Dots. *J. Phys. Chem. B* **2001**, *105*, 8861-8871.
- (12) Darbandi, M.; Thomann, R.; Nann, T. Single Quantum Dots in Silica Spheres by Microemulsion Synthesis. *Chem. Mater.* **2005**, *17*, 5720-5725.
- (13) Selvan, S. T.; Tan, T. T.; Ying, J. Y. Robust, Non-Cytotoxic, Silica-Coated CdSe Quantum Dots with Efficient Photoluminescence. *Adv. Mater.* **2005**, *17*, 1620-1625.
- (14) Santra, S.; Zhang, P.; Wang, K.; Tapeç, R.; Tan, W. Conjugation of Biomolecules with Luminophore-Doped Silica Nanoparticles for Photostable Biomarkers. *Anal. Chem.* **2001**, *73*, 4988-4993.
- (15) Bagwe, R. P.; Yang, C.; Hilliard, L. R.; Tan, W. Optimization of Dye-Doped Silica Nanoparticles Prepared Using a Reverse Microemulsion Method. *Langmuir* **2004**, *20*, 8336-8342.
- (16) Soares-Santos, P. C. R.; Nogueira, H. I. S.; Félix, V.; Drew, M. G. B.; Sa Ferreira, R. A.; Carlos, L. D.; Trindade, T. Novel Lanthanide Luminescent Materials Based on Complexes of 3-Hydroxypicolinic Acid and Silica Nanoparticles. *Chem. Mater.* **2003**, *15*, 100-108.
- (17) Sun, H.-T.; Yang, J.; Fujii, M.; Sakka, Y.; Zhu, Y.; Asahara, T.; Shirahata, N.; Li, M.; Bai, Z.; Li, J.-G.; Gao, H. Highly Fluorescent Silica-Coated Bismuth-Doped Aluminosilicate Nanoparticles for Near-Infrared Bioimaging. *Small* **2011**, *7*, 199-203.
- (18) Li, Z.; Zhang, Y. Monodisperse Silica-Coated Polyvinylpyrrolidone/NaYF<sub>4</sub> Nanocrystals with Multicolor Upconversion Fluorescence Emission. *Angew. Chem. Int. Ed.* **2006**, *45*, 7732-7735.
- (19) Sivakumar, S.; Diamente, P. R.; van Veggel, F. C. J. M. Silica-Coated Ln<sup>3+</sup>-Doped LaF<sub>3</sub> Nanoparticles as Robust Down- and Upconverting Biolabels. *Chem. Eur. J.* **2006**, *12*, 5878-5884.
- (20) Nagarajan, S.; Li, Z.; Marchi-Artzner, V.; Grasset, F.; Zhang, Y. Imaging Gap Junctions with Silica-Coated Upconversion Nanoparticles. *Med. Biol. Eng. Comput.* **2010**, *48*, 1033-1041.
- (21) Larson, D. R.; Ow, H.; Vishwasrao, H. D.; Heikal, A. A.; Wiesner, U.; Webb, W. W. Silica Nanoparticle Architecture Determines Radiative Properties of Encapsulated Fluorophores. *Chem. Mater.* **2008**, *20*, 2677-2684.
- (22) Lei, B.; Li, B.; Zhang, H.; Lu, S.; Zheng, Z.; Li, W.; Wang, Y. Mesostructured Silica Chemically Doped with RuII as a Superior Optical Oxygen Sensor. *Adv. Funct. Mater.* **2006**, *16*, 1883-1891.
- (23) Labéguerie-Egée, J.; McEvoy, H.; McDonagh, C. Synthesis, Characterisation and Functionalisation of Luminescent Silica Nanoparticles. *J. Nanopart. Res.* **2011**, *13*, 6455-6465.
- (24) Ma, D.; Kell, A. J.; Tan, S.; Jakubek, Z. J.; Simard, B. Photophysical Properties of Dye-Doped Silica Nanoparticles Bearing Different Types of Dye-Silica Interactions. *J. Phys. Chem. C* **2009**, *113*, 15974-15981.
- (25) Grasset, F.; Dorson, F.; Cordier, S.; Molard, Y.; Perrin, C.; Marie, A. M.; Sasaki, T.; Haneda, H.; Bando, Y.; Mortier, M. Water-in-Oil Microemulsion Preparation and Characterization of Cs<sub>2</sub>Mo<sub>6</sub>X<sub>14</sub>@SiO<sub>2</sub> Phosphor Nanoparticles Based on Transition Metal Clusters (X = Cl, Br, and I). *Adv. Mater.* **2008**, *20*, 143-148.
- (26) Aubert, T.; Grasset, F.; Mornet, S.; Duguet, E.; Cador, O.; Cordier, S.; Molard, Y.; Demange, V.; Mortier, M.; Haneda, H. Functional Silica Nanoparticles Synthesized by Water-in-Oil Microemulsion Processes. *J. Colloid Interface Sci.* **2010**, *341*, 201-208.
- (27) Aubert, T.; Ledneva, A. Y.; Grasset, F.; Kimoto, K.; Naumov, N. G.; Molard, Y.; Saito, N.; Haneda, H.; Cordier, S.

- Synthesis and Characterization of  $A_4[Re_6Q_8L_6]@SiO_2$  Red-Emitting Silica Nanoparticles Based on Re6 Metal Atom Clusters (A = Cs or K, Q = S or Se, and L = OH or CN). *Langmuir* **2010**, *26*, 18512-18518.
- (28) Grasset, F.; Dorson, F.; Molard, Y.; Cordier, S.; Demange, V.; Perrin, C.; Marchi-Artzner, V.; Haneda, H. One-Pot Synthesis and Characterizations of Bi-Functional Phosphor-Magnetic  $@SiO_2$  Nanoparticles: Controlled and Structured Association of Mo-6 Cluster Units and Gamma-Fe<sub>2</sub>O<sub>3</sub> Nanocrystals. *Chem. Commun.* **2008**, 4729-4731.
- (29) Cordier, S.; Kirakci, K.; Méry, D.; Perrin, C.; Astruc, D. Nanocluster Cores (X = Br, I): From Inorganic Solid State Compounds to Hybrids. *Inorg. Chim. Acta* **2006**, *359*, 1705-1709.
- (30) Dorman, W. C.; McCarley, R. E. Chemistry of the Polynuclear Metal Halides. XII. Preparation of Molybdenum and Tungsten M<sub>6</sub>X<sub>8</sub><sup>+</sup> Clusters by Reduction of Higher Halides in Molten Sodium Halide-Aluminum Halide Mixtures. *Inorg. Chem.* **1974**, *13*, 491-493.
- (31) Szczepura, L. F.; Ketcham, K. A.; Ooro, B. A.; Edwards, J. A.; Templeton, J. N.; Cedeño, D. L.; Jircitano, A. J. Synthesis and Study of Hexanuclear Molybdenum Clusters Containing Thiolate Ligands. *Inorg. Chem.* **2008**, *47*, 7271-7278.
- (32) Golden, J. H.; Deng, H.; DiSalvo, F. J.; Fréchet, J. M. J.; Thompson, P. M. Monodisperse Metal Clusters 10 Angstroms in Diameter in a Polymeric Host: The "Monomer as Solvent" Approach. *Science* **1995**, *268*, 1463-1466.
- (33) Prabusankar, G.; Molard, Y.; Cordier, S.; Golhen, S.; Gal, Y. L.; Perrin, C.; Ouahab, L.; Kahlal, S.; Halet, J.-F. Experimental and Theoretical Evidence of pi-d Interactions in Supramolecular Assemblies Based on TTF-CH=CH-Py Ligands Tethered to Mo<sub>6</sub>Xi<sub>8</sub> Octahedral Molybdenum Halide Cluster Cores. *Eur. J. Inorg. Chem.* **2009**, 2153-2161.
- (34) Méry, D.; Ornelas, C.; Daniel, M.-C.; Ruiz, J.; Rodrigues, J.; Astruc, D.; Cordier, S.; Kirakci, K.; Perrin, C. Mo<sub>6</sub>Br<sub>8</sub>-Cluster-Cored Organometallic Stars and Dendrimers. *C. R. Chim.* **2005**, *8*, 1789-1797.
- (35) Ababou-Girard, S.; Cordier, S.; Fabre, B.; Molard, Y.; Perrin, C. Assembly of Hexamolybdenum Metallic Clusters on Silicon Surfaces. *ChemPhysChem* **2007**, *8*, 2086-2090.
- (36) Fabre, B.; Cordier, S. p.; Molard, Y.; Perrin, C.; Ababou-Girard, S.; Godet, C. Electrochemical and Charge Transport Behavior of Molybdenum-Based Metallic Cluster Layers Immobilized on Modified n- and p-Type Si(111) Surfaces. *J. Phys. Chem. C* **2009**, *113*, 17437-17446.
- (37) Molard, Y.; Dorson, F.; Circu, V.; Roisnel, T.; Artzner, F.; Cordier, S. Clustomesogens: Liquid Crystal Materials Containing Transition-Metal Clusters. *Angew. Chem. Int. Ed.* **2010**, *49*, 3351-3355.
- (38) Molard, Y.; Dorson, F.; Brylev, Konstantin A.; Shestopalov, Michael A.; Le Gal, Y.; Cordier, S.; Mironov, Yuri V.; Kitamura, N.; Perrin, C. Red-NIR Luminescent Hybrid Poly(methyl methacrylate) Containing Covalently Linked Octahedral Rhenium Metallic Clusters. *Chem. Eur. J.* **2010**, *16*, 5613-5619.
- (39) Kirakci, K.; Kubát, P.; Dušek, M.; Fejfarová, K.; Šícha, V.; Mosinger, J.; Lang, K. A Highly Luminescent Hexanuclear Molybdenum Cluster - A Promising Candidate toward Photoactive Materials. *Eur. J. Inorg. Chem.* **2012**, *2012*, 3107-3111.
- (40) Kirakci, K.; Cordier, S.; Perrin, C. Synthesis and Characterization of Cs<sub>2</sub>Mo<sub>6</sub>X<sub>14</sub> (X = Br or I) Hexamolybdenum Cluster Halides: Efficient Mo<sub>6</sub> Cluster Precursors for Solution Chemistry Syntheses. *Z. Anorg. Allg. Chem.* **2005**, *631*, 411-416.
- (41) Maverick, A. W.; Najdzionek, J. S.; MacKenzie, D.; Nocera, D. G.; Gray, H. B. Spectroscopic, Electrochemical, and Photochemical Properties of Molybdenum(II) and Tungsten(II) Halide Clusters. *J. Am. Chem. Soc.* **1983**, *105*, 1878-1882.
- (42) Jackson, J. A.; Turro, C.; Newsham, M. D.; Nocera, D. G. Oxygen Quenching of Electronically Excited Hexanuclear Molybdenum and Tungsten Halide Clusters. *J. Phys. Chem.* **1990**, *94*, 4500-4507.
- (43) Gao, L.; Peay, M. A.; Gray, T. G. Encapsulation of Phosphine-Terminated Rhenium(III) Chalcogenide Clusters in Silica Nanoparticles. *Chem. Mater.* **2010**, *22*, 6240-6245.
- (44) Aubert, T.; Burel, A.; Esnault, M.-A.; Cordier, S.; Grasset, F.; Cabello-Hurtado, F. Root Uptake and Phytotoxicity of Nanosized Molybdenum Octahedral Clusters. *J. Hazard. Mater.* **2012**, *219-220*, 111-118.
- (45) Leonardelli, S.; Facchini, L.; Fretigny, C.; Tougne, P.; Legrand, A. P. Silicon-29 NMR Study of Silica. *J. Am. Chem. Soc.* **1992**, *114*, 6412-6418.
- (46) Sheldon, J. C. Bromo- and Iodo-molybdenum(ii) Compounds. *J. Chem. Soc.* **1962**, 410-415.
- (47) Robinson, L. M.; Lu, H.; Hupp, J. T.; Shriver, D. F. Nature of the Interaction and Photophysical Properties of [Mo<sub>6</sub>Cl<sub>8</sub>(SO<sub>3</sub>CF<sub>3</sub>)<sub>6</sub>]<sup>2-</sup> and [Mo<sub>6</sub>Cl<sub>8</sub>Cl<sub>6</sub>]<sup>2-</sup> on Silica Gel. *Chem. Mater.* **1995**, *7*, 43-49.
- (48) Triantaphylidés, C.; Havaux, M. Singlet Oxygen in Plants: Production, Detoxification and Signaling. *Trends Plant Sci.* **2009**, *14*, 219-228.
- (49) Radu, M.; Munteanu, M. C.; Petrache, S.; Serban, A.; Dinu, D.; Hermenean, A.; Sima, C.; Dinischiotu, A. Depletion of Intracellular Glutathione and Increased Lipid Peroxidation Mediate Cytotoxicity of Hematite Nanoparticles in MRC-5 Cells. *Acta Biochim. Pol.* **2010**, *57*, 355-360.
- (50) McCarthy, J.; Inkiewicz-Stępnik, I.; Corbalan, J. J.; Radomski, M. W. Mechanisms of Toxicity of Amorphous Silica Nanoparticles on Human Lung Submucosal Cells in Vitro: Protective Effects of Fisetin. *Chem. Res. Toxicol.* **2012**, *25*, 2227-2235.
- (51) Lison, D.; Thomassen, L. C. J.; Rabolli, V.; Gonzalez, L.; Napierska, D.; Seo, J. W.; Kirsch-Volders, M.; Hoet, P.; Kirschhock, C. E. A.; Martens, J. A. Nominal and Effective Dosimetry of Silica Nanoparticles in Cytotoxicity Assays. *Toxicol. Sci.* **2008**, *104*, 155-162.

Insert Table of Contents artwork here

